Characterization of the radiation background at the Spallation Neutron Source

Douglas D. DiJulio[1,2], Nataliia Cherkashyna[1], Julius Scherzinger[1,2], Anton Khaplanov[1], Dorothea Pfeiffer[1,3], Carsten P. Cooper-Jensen[1,4], Kevin G. Fissum[1,2], Kalliopi Kanaki[1], Oliver Kirstein[1,5], Georg Ehlers[6], Franz X. Gallmeier[7], Donald E. Hornbach[7], Erik B. Iverson[7], Robert J. Newby[7], Richard J. Hall-Wilton[1,8], Phillip M. Bentley[1,4]

[1] European Spallation Source ERIC, SE-221 00 Lund, Sweden
[2] Division of Nuclear Physics, Lund University, SE-221 00 Lund, Sweden
[3] CERN, CH-1211 Geneva 23, Switzerland
[4] Department of Physics and Astronomy, Uppsala University, 751 05 Uppsala, Sweden
[5] University of Newcastle, Callaghan, NSW 2308, Australia
[6] Quantum Condensed Matter Division, ORNL, Oak Ridge TN-37831, USA
[7] Instrument and Source Division, ORNL, Oak Ridge, TN-37831, USA
[8] Mid-Sweden University, SE-851 70 Sundsvall, Sweden

E-mail: douglas.dijulio@esss.se

Abstract. We present a survey of the radiation background at the Spallation Neutron Source (SNS) at Oak Ridge National Laboratory, TN, USA during routine daily operation. A broad range of detectors was used to characterize primarily the neutron and photon fields throughout the facility. These include a WENDI-2 extended range dosimeter, a thermoscientific NRD, an Arktis ^{4}He detector, and a standard NaI photon detector. The information gathered from the detectors was used to map out the neutron dose rates throughout the facility and also the neutron dose rate and flux profiles of several different beamlines. The survey provides detailed information useful for developing future shielding concepts at spallation neutron sources, such as the European Spallation Source (ESS), currently under construction in Lund, Sweden.

1. Introduction

Spallation neutron sources provide scientists with intense fluxes of cold and thermal neutrons for condensed matter investigations. The usable signal for such experiments is typically on the order of a few meVs. However, at a spallation neutron source, the experiments may also be contaminated by the presence of a significant number of high-energy neutrons, which can extend up to the energy of the primary proton beam (several GeVs). These neutrons are generated in the primary spallation target and can reach the experimental stations via a number of mechanisms, which may include streaming down the neutron guides, penetration through the target biological shielding, or leakage from a nearby beamline. The presence of the these neutrons causes significant shielding concerns at spallation sources which are not otherwise present at reactor-based facilities [1, 2, 3]. Additionally, at a pulsed spallation source the high-energy neutrons are correlated with the proton impact on the spallation target and may show up as a prompt-pulse of particles arriving at the sample position of a particular instrument [4, 5]. This is particularly

important for inelastic scattering instruments, where signals may be on the order of 10^{-6}-10^{-4} compared to elastic scattering [6]. Two such instruments relevant to the current study are the hybrid spectrometer (HYSPEC) and the cold neutron spectrometer (CNCS) instruments [7, 8], which both exhibit noticeable prompt-pulse signals [4, 9].

Understanding the mechanisms which give rise to the high-energy prompt-pulse backgrounds at modern spallation sources can provide valuable information for upcoming sources, such as the the European Spallation Source (ESS) [10], currently under construction in Lund, Sweden. Therefore, we have carried out a survey of the radiation background at the Spallation Neutron Source (SNS) at Oak Ridge National Laboratory, TN, USA during routine daily operation [11]. The measurements were carried out around the target monolith, close to the shielding of beamlines, and on cracks between shielding blocks. A broad range of detectors, including some which are not traditionally used at spallation neutron sources for background characterization, were employed. The advantages of these types of detectors, particularly for high-energy neutron detection, will be discussed below.

In the following, we present some relevant information on the shielding configurations at SNS, the methods and results of our measurements, and lastly some discussion and conclusions with the focus in particular on backgrounds primarily related to neutron and photon fields measured throughout the facility.

2. The SNS facility

The SNS is an accelerator-based facility with a proton beam of 1 GeV that is incident on a mercury target. The neutrons are moderated by three cryogenic hydrogen moderators and one ambient water moderator. The moderators are surrounded by a water cooled beryllium and steel reflector region. The biological shielding consists of approximately 5 m of iron and 1 m of high-density concrete. High-density concretes contain aggregates, such as magnetite, which are more efficient for shielding against high-energy neutrons above 1 MeV and γ-rays compared to standard concrete. In total there are 18 beamlines extending from the shielding. A detailed overview of the target station design can be found in Ref. [12].

At SNS, the neutron beamlines can be straight or curved, where the latter geometry is used to reduce the amount of high-energy particles reaching the sample position of an instrument. Each beamline has a primary shutter inside the monolith, in order to stop the incident radiation and allow access into the instrument caves during daily operation. The shutters are designed to comprise of a 1 meter long block of tungsten surrounded by steel [13]. Many beamlines also have secondary shutters, which makes it possible for multiple beamlines to share a single primary shutter [14]. The standard shielding materials for beamlines include regular concrete, steel, and high-density concrete. Depending on the particular geometrical layout of the beamline, shielding thicknesses can reach up to 2 m of regular concrete [15]. Shielding challenges at SNS have been highlighted in a number of previous publications [13, 15] and specific beamline calculations can also be found in [14, 16].

3. Equipment

The measurements were carried out at SNS using a wide range of detectors. Each detector will be briefly presented and described below. Detailed descriptions will be referenced for further information.

3.1. Neutron dosimetry

The neutron dose rates at SNS were mapped with a WENDI-2 (<5 GeV) [17] dosimeter and a Thermoscientific NRD (<10 MeV) [18]. The WENDI-2 is a cylindrical dosimeter containing a ^{3}He tube surrounded by a tungsten loaded polyethylene shell. The tungsten powder layer is 1.5 cm thick and provides a scattering layer with a large interaction probability above ∼10 MeV, ultimately maintaining the sensitivity of the device at higher energies. On the other hand, the NRD is a spherical dosimeter loaded with cadmium and has a decreasing sensitivity above ∼10 MeV. Thus measurements with the two dosimeters at the same locations may reveal areas where the the fast neutron dose above ∼10 MeV is significant. The NRD is limited to dose rates above 0.2 μSv/hr [18] while the WENDI-2 is limited to dose rates above 0.001 μSv/hr [17]. The calibration of the two dosimeters was checked against a ^{252}Cf source, which emits neutrons predominately in the energy region where the response of the dosimeters is nearly identical. A maximum difference of ∼20% in the measured dose rates with WENDI-2 and NRD was observed.

3.2. Fast-neutron detection

The Neutron Diagnostic Tool (NDT) from Arktis Radiation Detectors [19, 20, 21, 22] was used to measure the fast-neutron rates throughout the facility. The noble gas scintillation counter NDT was developed for fast neutron counting in high γ-ray background environments and is optimized for neutron energies between 0.5 MeV and 20 MeV. The active detector volume is 1.05 liters of highly pressurized (179 bar) ^{4}He gas in a 2 inch inner diameter steel tube. The ultraviolet scintillation light is shifted to longer wavelengths by a wavelength shifting coating on the reflecting sides of the tube. The transmitted light is read out using two R580 Hamamatsu [23] photo-multiplier-tubes (PMTs). The PMTs are operated in photon-counting mode and the pulses are processed by a 10 bit WaveDREAM-B16 [21] digitizer with a sampling rate of 1 GS/s. This set-up allows for combined neutron/γ-ray count rates of up to 1 MHz, identification of fast neutrons by both pulse-shape and pulse-height discrimination, and the determination of the interaction point along the active volume of the detector [22]. Rejection of the γ-ray events is made possible by the fact that high-pressure ^{4}He scintillation light exhibits fast and slow components, with decay times of a few nanoseconds and about 1 ms respectively [20]. These decay constants are attributed to the singlet and triplet states of the excited dimers formed by the excitation of atomic ^{4}He. The relative strength of the fast component to the total light yields enables the identification of incident particles by discriminating recoiling electrons correlated to γ-ray events and recoiling alpha particles correlated to neutrons.

The count rates collected by the NDT were converted to fast-neutron count rates for further analysis. For this, a correction for the non-uniform light transport to the PMTs was applied. The non-uniformity is due to light loss in the defuse reflector. The reflector is a thin teflon (PTFE) coating which has normally a high reflectivity (∼90%) for visible light. On top of this is also a phosphor coating to shift the wavelength from 80 nm (emission from He) to 430 nm (PMT sensitivity). This means that for the long distance (50 cm) from the center of the detector to the PMTs, a significant fraction of light will be lost by transmission/absorption in the reflector material. The effect of the reflector is the main light-loss mechanism in the detector. The interaction position was calculated as the relative difference between the numbers of photons counted in the right PMT and in the left PMT divided by the total photon number. The maximum photon count was a function strongly dependent on the interaction point and the detection efficiency of the detector is therefore also dependent on the interaction point. In order to calculate the neutron rate, the neutron interaction efficiency was estimated to be 0.03 for the energy range between 0.5 MeV and 20 MeV and zero for all other energies. For 0.5 MeV to 6 MeV, the values were corrected for gas pressure from Ref. [20] and were used in the analysis. An average efficiency of 0.02 was estimated from Evaluated Nuclear Data Files (ENDF) cross

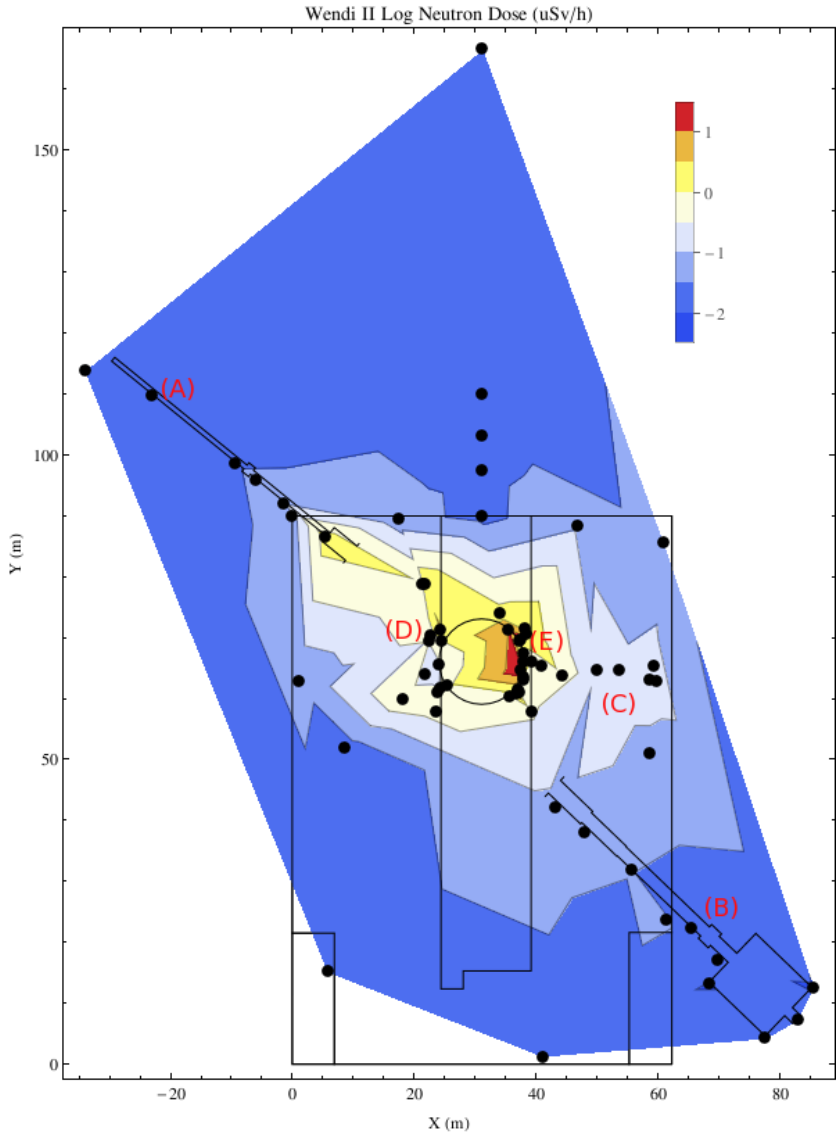

Figure 1: Contour plot of the neutron dose rate measurements carried out with the WENDI-2 dosimeter. The black dots represent the measurement points and the marked letter regions highlight several areas of interest, as described in the text.

sections [24] and the calculations from Ref. [20] for energies above 6 MeV.

3.3. γ-ray spectroscopy

A large (5x10x40cm^3) NaI detector was used for γ-ray measurements throughout the facility. The resolution of the NaI detector was not sufficient to separate the 511 keV annihilation peak from the often-present 478 keV peak, due to neutron capture on ^{10}B, which is common at neutron scattering facilities. However, the advantage of the NaI detector was its considerably large efficiency at high energies.

Table 1: Comparison between the measured and calculated neutron dose rates from the WENDI-2, NRD, and the Arktis NDT at several measurement locations throughout the area shown in Fig. 1. The letters indicate the regions where the measurements were carried out. The measured Arktis NDT count rates are also given for completeness.

Position (Region Fig. 1)	WENDI-2 (μSv hr^{-1})	NRD (μSv hr^{-1})	Arktis NDT (μSv hr^{-1})	Arktis NDT (n s^{-1}cm^{-2})
1 (C)	0.11(2)	0.44(14)	0.28(1)	0.45(2)
2 (D)	0.78(14)	0.87(29)	0.93(7)	1.48(10)
3 (D)	3.27(19)	4.37(144)	x	x
4 (D)	0.94(14)	x	0.97(12)	1.56(19)
5 (D)	2.95(21)	2.62(86)	5.82(28)	9.28(45)
6 (E)	21.85(122)	9.61(317)	28.68(63)	45.78(101)
7 (E)	10.08(79)	8.67(108)	14.71(45)	23.49(72)
8 (E)	0.92(12)	0.57(16)	1.36(14)	2.17(22)
9 (E)	0.95(12)	0.89(38)	1.43(14)	2.29(23)

4. Results and Discussion

Fig. 1 shows a neutron dose rate contour map collected with the WENDI-2 dosimeter. The indicated points represent the measurement locations and the dose rates were calculated by averaging the collected data over periods when the proton beam was stable. The central circular and rectangular regions in the middle of the map mark the edges of the biological shielding of the target monolith. The letter markers on the map indicate several regions of interest. Point (A) highlights the backscattering spectrometer BASIS [25], point (B) the powder diffractometer POWGEN [26], point (C) is an area down on the instrument floor between the shielding of the HYSPEC and FNPB [27] beamlines, and points (D) and (E) are regions where the instrument beamline shielding meets the target monolith shielding. The highest dose rate measured with the WENDI-2 was $\sim$25 μSv/hr, indicated by the red color in the map, which was in region (E) on top of a gap between an instrument shielding block and the monolith wall.

Table 1 presents a comparative study of the WENDI-2, NRD, and Arktis NDT dose rates from the measurements throughout the facility. The regions where the specified measurements were taken are indicated in the table. The Arktis NDT dose rates were calculated from the collected count rates and using a dose conversion factor of 0.000174 μSv cm^2 [28]. This is the dose conversion factor for 1 MeV neutrons, which corresponds to the maximum in the cross-section for ^{4}He neutron elastic scattering [20]. The broad agreement between the measured and calculated dose rates may support the conclusion that the dose rates arise from neutrons around 1 MeV at the selected positions. However, it should be mentioned that further comparison of the detector results requires more details regarding the response functions of the detectors, systematic uncertainties and information about the local radiation fields. Detailed simulations would also be of great value for the analysis of the current results.

In areas where beamlines are present, geometrical effects may play an important role in how the dose rate scales as a distance along the beamline. To investigate this further, we also performed measurements along specific beamlines. Fig. 2 presents the dose rates measured along the two beamlines POWGEN and BASIS with the WENDI-2 dosimeter. The dose rate measured along the straight beamline (POWGEN) was fit by a straight line and the dose rate measured along the curved beamline (BASIS) was fit with a $1/r$ function.

Similar measurements were also carried out along the HYSPEC and TOPAZ [29] beamlines

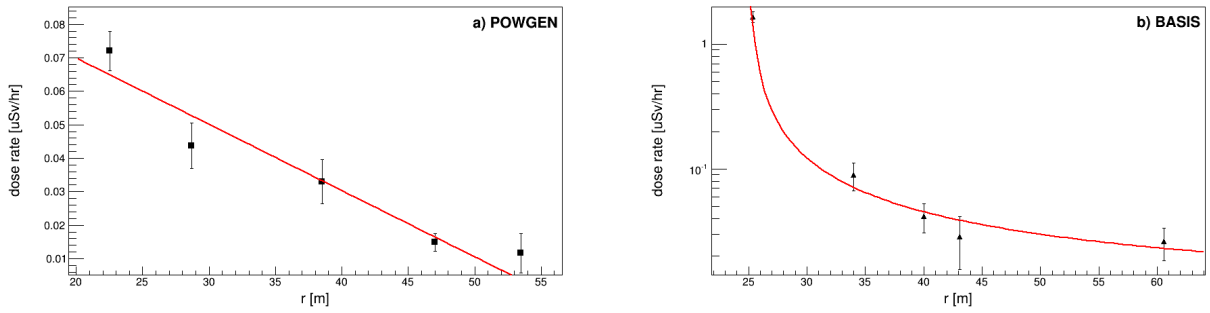

Figure 2: Neutron dose rates measured with the WENDI-2 dosimeter along the a) POWGEN and b) BASIS instruments as a function of distance from the monolith biological shielding.

using the Arktis NDT and the results are shown in Fig. 3. The two beamlines are in the same vicinity and both curves were fit with $1/r^2$ functions.

Fig. 4 presents the data collected based on traces taken with a scope and the NaI detector. The measurements were taken on the instrument beamline shielding above a gap in the shielding and close to the biological shield of the monolith. Each trace was 20 ms long and has one million samples at 20 ns intervals. The data contains 400 traces. The scope triggered randomly, but this usually happened in the beginning of an SNS pulse. Traces where this was not the case were manually removed and amounted to approximately 10% of the total. Each event contained an amplitude and a time signal. Overall, there were 72k events in the data set.

The left panel of Fig. 4 shows the number of counts collected as a function of time. The prompt-pulse is clearly visible with the repetition rate of 60 hz. The right panel shows a two-dimensional scatter plot of the amplitude vs the time. The spectra have three noticeable components. The activation γ-rays are always present and occur in the lowest amplitudes. Capture γ-rays occur up to about 0.01 V, which corresponds to $\sim$10 MeV, and this contribution dies off after a few ms. Lastly, there are the prompt γ-ray events which occur only in the beginning of the pulse, which is visible with the repetition rate of 60 hz. These have much higher energies than 10 MeV. However, it can be noted that pulse-pile up effects may contribute to a fraction of the large observed amplitudes due to the high instantaneous rate. This last energy group of photons represents an interesting possible contribution to the prompt-pulse background unique to pulsed spallation sources. High-energy photons coincident with the proton beam can lead to additional neutrons generated by photonuclear reactions through the giant dipole resonance. These neutrons have higher energies, into the MeV range, and can travel into and induce additional secondaries in the surrounding instrument shielding. The importance of this contribution to background noise at spallation neutron facilities requires more detailed investigations.

5. Conclusions and Outlook

In summary, we carried out measurements at the SNS during routine user operation in order to understand the radiation leaking from the shielding structures. We presented maps of the neutron dose rate throughout the facility and also along various neutron beamlines. These highlight potential future enhancements in shielding solutions and also differences in the leakage properties of the the individual beamlines. A comparative study between the neutron detectors suggested that the dose rates around the facility at selected positions may be contributed to neutrons on the order of 1 MeV. Lastly, our results indicated the presence of high-energy photons

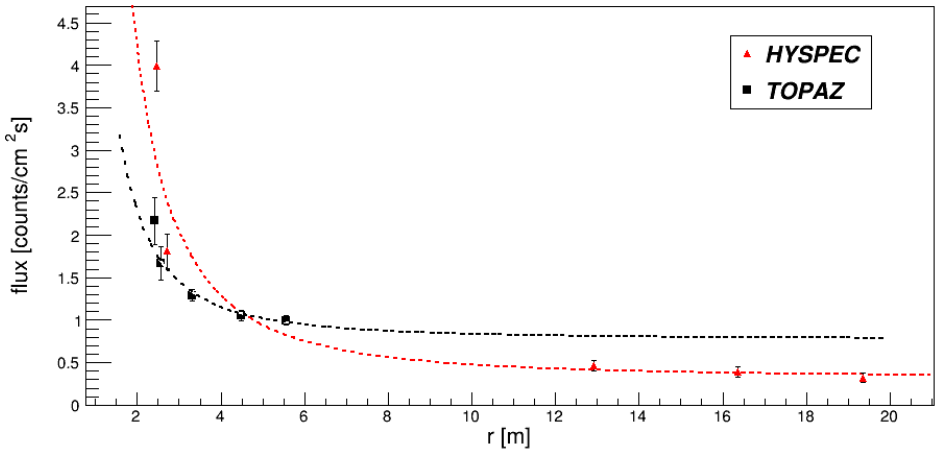

Figure 3: Neutron fluxes measured with the Arktis NDT as a function of distance from the monolith biological shielding for the HYSPEC and TOPAZ beamlines.

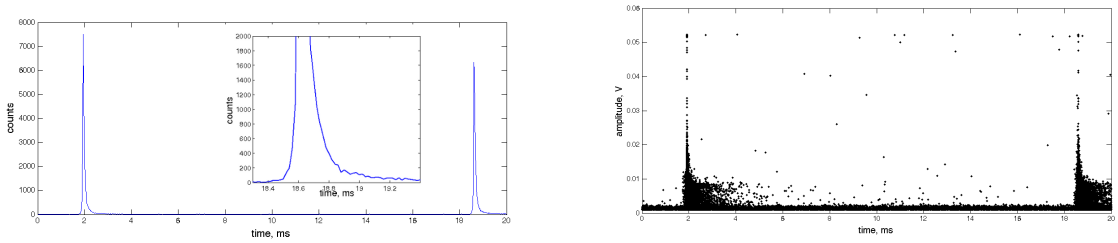

(a) (b)

Figure 4: Panel a) shows the number of counts as a function of time collected with the NaI detector for a position on top of the instrument shielding close to the monolith wall. The prompt-pulse is clearly visible every 60 hz. Panel b) shows a scatter plot of the amplitude as a function of time collected with the NaI detector. Prompt γ-rays, capture γ-rays, and γ-rays from continuous activation make up the three major components.

correlated with the primary beam impact on target on top of the instrument shielding.

The results presented in this paper highlight the need for an improved understanding of backgrounds at modern spallation neutron source facilities. Future studies could for example include an analysis of correlations between the measurements and the status of the beamline shutters throughout the facility, detailed modeling of the response functions of the detectors and local radiation fields, and also the implementation of detectors which can provide more precise determination of the energy of the neutrons leaking from the shielding components.

6. Acknowledgments

The authors would like to thank the Nuclear and Radiological Support Services staff at SNS for assisting in the measurements at the facility. We would also like to thank Professor Lawrence Weinstein and the Experimental Nuclear and Particle Physics Group of Old Dominion University for providing detectors and electronics for our measurements at short notice. This research at ORNL's Spallation Neutron Source was supported by the Scientific User Facilities Division,

Office of Basic Energy Sciences, U.S. Department of Energy.

References

[1] Russel G *et al.* 1988 Proceedings of the ICANS-X Conference Los Alamos, NM
[2] Koprivnikar I and Schachinger E 2002 *Nucl. Instrum. and Meth. in Phys. Res. A* **487** 571
[3] Cherkashyna N *et al.* 2015 *Physical Review Special Topics: Accelerators and Beams* **18** 083501
[4] Cherkashyna N *et al.* 2014 *Journal of Physics: Conference Series* **528** 012013
[5] Cherkashyna N *et al.* 2015 Submitted to the Proceedings of ICANS XXI (International Collaboration on Advanced Neutron Sources) Mito, Japan
[6] Kajimoto R *et al.* 2013 *J. Phys. Soc. Jpn.* **82** SA032
[7] Winn, Barry, Filges, Uwe, Garlea, V Ovidiu, Graves-Brook, Melissa, Hagen, Mark, Jiang, Chenyang, Kenzelmann, Michel, Passell, Larry, Shapiro, Stephen M, Tong, Xin and Zaliznyak, Igor 2015 *EPJ Web of Conferences* **83** 03017 URL `http://dx.doi.org/10.1051/epjconf/20158303017`
[8] Ehlers G, Podlesnyak A A, Niedziela J L, Iverson E B and Sokol P E 2011 *Review of Scientific Instruments* **82** 085108 ISSN 00346748 URL `http://dx.doi.org/doi/10.1063/1.3626935`
[9] Winn B and Hagen M 2012 Inelastic spurion from the prompt pulse, HYSPEC memo hyspec_memo01272012_01 http://neutrons.phy.bnl.gov/HYSPEC/memos_technical_reports.shtm
[10] Peggs S *et al.* 2013 ESS Technical Design Report Lund, Sweden
[11] Mason T E, Abernathy D, Anderson I, Ankner J, Egami T, Ehlers G, Ekkebus A, Granroth G, Hagen M, Herwig K, Hodges J, Hoffmann C, Horak C, Horton L, Klose F, Larese J, Mesecar A, Myles D, Neuefeind J, Ohl M, Tulk C, Wang X L and Zhao J 2006 *Phys. B (Amsterdam, Neth.)* **385-386** 955–960
[12] Haines J *et al.* 2014 *Nucl. Instrum. and Meth. in Phys. Res. A* **764** 94
[13] Ferguson P *et al.* 2005 *Rad. Prot. Dos.* **115** 170
[14] Popiva I *et al.* 2014 *Prog. Nucl. Sci. and Tech.* **4** 753
[15] Gallmeier F *et al.* 2005 *Rad. Prot. Dos.* **115** 23
[16] Popiva I and Gallmeier F 2014 *Prog. Nucl. Sci. and Tech.* **4** 178
[17] Olsher R *et al.* 2000 *Health Physics* **79 (2)** 170–181
[18] ASP-2e/NRD Portable Neutron REM Meter. `http://www.thermoscientific.com`
[19] Arktis Radaition Detectors `http://www.arktis-detectors.com`
[20] Chandra R *et al.* 2012 *Journal of Instrumentation* **7** C03035
[21] Friederich H *et al.* 2012 *Real Time Conference (RT), 2012 18th IEEE-NPSS* pp 1–7
[22] Chandra R *et al.* 2010 *2010 IEEE International Conference on Technologies for Homeland Security (HST)* 410 – 413
[23] Hamamatsu Photonics K.K. `http://www.hamamatsu.com`
[24] ENDF: Evaluated Nuclear Data File `https://www-nds.iaea.org/exfor/endf.htm`
[25] Mamontov E and Herwig K W 2011 *Review of Scientific Instruments* **82** 085109 URL `http://scitation.aip.org/content/aip/journal/rsi/82/8/10.1063/1.3626214`
[26] The Powder Diffractometer at SNS http://neutrons.ornl.gov/powgen/
[27] Fundamental Neutron Physics Beamline at SNS http://neutrons.ornl.gov/fnpb/
[28] ICRP Publication 116 2010, Annals of the ICRP Vol. 40 Nos 2-5
[29] TOPAZ: The Single-Crystal Diffractometer at SNS http://neutrons.ornl.gov/topaz/